

# Simultaneous determination of thermal conductivity, thermal diffusivity and specific heat in sI methane hydrate

W. F. Waite,<sup>1</sup> L. A. Stern,<sup>2</sup> S. H. Kirby,<sup>2</sup> W. J. Winters<sup>1</sup> and D. H. Mason<sup>1</sup>

<sup>1</sup>U.S. Geological Survey, 384 Woods Hole Road, Woods Hole, MA 02543, USA. E-mail: wwaite@usgs.gov

<sup>2</sup>U.S. Geological Survey, 345 Middlefield Rd., MS 977, Menlo Park, CA 94025, USA

Accepted 2007 January 17. Received 2007 January 17; in original form 2006 October 30

## SUMMARY

Thermal conductivity, thermal diffusivity and specific heat of sI methane hydrate were measured as functions of temperature and pressure using a needle probe technique. The temperature dependence was measured between  $-20^{\circ}\text{C}$  and  $17^{\circ}\text{C}$  at 31.5 MPa. The pressure dependence was measured between 31.5 and 102 MPa at  $14.4^{\circ}\text{C}$ . Only weak temperature and pressure dependencies were observed. Methane hydrate thermal conductivity differs from that of water by less than 10 per cent, too little to provide a sensitive measure of hydrate content in water-saturated systems. Thermal diffusivity of methane hydrate is more than twice that of water, however, and its specific heat is about half that of water. Thus, when drilling into or through hydrate-rich sediment, heat from the borehole can raise the formation temperature more than 20 per cent faster than if the formation's pore space contains only water. Thermal properties of methane hydrate should be considered in safety and economic assessments of hydrate-bearing sediment.

**Key words.** methane hydrate, specific heat, thermal conductivity, thermal diffusivity.

## INTRODUCTION

Gas hydrates are crystalline solids in which molecules of a 'guest' species occupy and stabilize cages formed by water molecules. Methane,  $\text{CH}_4$ , is the most common naturally occurring guest species;  $\text{CH}_4$  hydrate is found in shallow permafrost and continental margin sediments worldwide (Kvenvolden 2000). The United States alone has an estimated  $5665 \text{ Tm}^3$  (Sloan 2004) to  $9000 \text{ Tm}^3$  (Collett 1995) of  $\text{CH}_4$  bound in hydrate. Though only a fraction of the total methane in hydrate will likely be economically accessible as an energy resource (Kerr 2004), the vast quantity and geospatial extent of methane hydrate, coupled with the sensitive dependence of  $\text{CH}_4$  hydrate stability on temperature, give rise to environmental considerations of local, regional and global scope (see references in Xu & Germanovich 2006).

The response of  $\text{CH}_4$  hydrate to a changing thermal environment is controlled by its thermal conductivity,  $\lambda$ , thermal diffusivity,  $\kappa$  and specific heat,  $c_p$ . These properties are described succinctly by Briaud & Chaouch (1997): 'A high value of thermal conductivity means heat travels easily through the material; a high value of specific heat means that it takes a lot of heat to raise the temperature of the material; and a high value of diffusivity means that it will take little time for the temperature to rise in the material'.

On localized length scales, thermal diffusivity and specific heat of  $\text{CH}_4$  hydrate are important not only for modelling controlled production of  $\text{CH}_4$  from hydrate (Ji *et al.* 2003; Pooladi-Darvish 2004; Hong & Pooladi-Darvish 2005; Kurihara *et al.* 2005; Moridis

*et al.* 2005), but for hazard mitigation in conventional hydrocarbon extraction, which can destabilize hydrate underlying production equipment (Briaud & Chaouch 1997; Moridis & Kowalsky 2006). On local and regional scales, hydrate thermal conductivity is used in heat flow measurements (Grevemeyer & Villinger 2001; Hennings & Huenges 2005). Globally, hydrate thermal properties are needed to relate climate variability to  $\text{CH}_4$  released from hydrate (Dickens *et al.* 1995; Revil 2000).

Published  $\text{CH}_4$  hydrate thermal property measurements are rare, however, and seldom reported for temperatures appropriate for terrestrial hydrate occurrences. We provide fit equations for  $\lambda$ ,  $\kappa$  and  $c_p$ , measured in  $\text{CH}_4$  hydrate over the terrestrially relevant ranges of  $-20^{\circ}\text{C}$  to  $17^{\circ}\text{C}$  and 31.5 to 102 MPa. We then compare the effect of pore space  $\text{CH}_4$  hydrate, relative to water, on the bulk thermal properties of sediment.

## METHODS

### Theory

The method for simultaneously determining  $\lambda$ ,  $\kappa$  and  $c_p$  is given in Waite *et al.* (2006), along with needle probe measurements showing the expected literature results are obtained within our stated uncertainty for ice Ih and sII tetrahydrofuran (THF) hydrate. Here we summarize our needle-probe measurement technique, an extension of the von Herzen and Maxwell (1959) technique. A constant

current,  $I$ , is supplied to a heater wire with resistance,  $R$ , per meter. The heater wire's output per meter,  $Q$ , is determined from  $Q = 2I^2R$ , where the factor 2 accounts for the heater wire being a loop running the length of the needle probe. From Blackwell (1954), the heater wire's output causes the temperature change measured within the probe,  $\Delta T$ , to vary as:

$$\Delta T = A \ln(t) + B, \quad (1)$$

where  $t$  is the time in seconds since the probe began heating the sample. Thermal conductivity,  $\lambda$ , is calculated from the eq. (1) slope,  $A$ :

$$\lambda = \frac{1}{A} \cdot \frac{Q}{4\pi}. \quad (2)$$

Thermal diffusivity,  $\kappa$ , is calculated from the eq. (1) slope,  $A$ , and intercept,  $B$ :

$$\kappa = \left( \frac{r_p^2}{4} \right) \cdot \exp \left[ \frac{B}{A} + \gamma - \frac{2\pi\lambda}{H} \right], \quad (3)$$

where  $r_p$  is the probe radius, 0.8 mm and  $\gamma$  is Euler's constant, 0.5772.  $H$  describes the thermal contact between probe and sample, determined from:

$$H = Q \cdot \frac{Z_2}{Z_1}, \quad (4)$$

where  $Z_1$  and  $Z_2$  are fit parameters for the initial, transient dependence of  $\Delta T$  on time (Blackwell 1954):

$$\Delta T = Z_1 \cdot t - Z_1 \cdot Z_2 \cdot t^2 + Z_1 \cdot Z_2 \cdot Z_3 \cdot t^{2.5}. \quad (5)$$

Generally,  $t = 0$  is taken to be the moment current is first applied to the heater wire. Eq. 5, however, assumes  $t = 0$  when the probe first begins heating the sample. Because the initial transient temperature change lasts only  $\sim 2$  s in hydrate, the finite time delay between applying current to the needle probe's heater wire and the time at which the probe begins heating the sample cannot be ignored (Hammerschmidt 2005). This delay must be determined via calibration, as described in Waite *et al.* (2006).

Once  $\lambda$  and  $\kappa$  have been measured, specific heat,  $c_p$ , is calculated by solving the definition of  $\kappa$  (Kittel & Kroemer 1980) for  $c_p$ :

$$c_p \equiv \frac{\lambda}{\rho \cdot \kappa}, \quad (6)$$

where  $\rho$  is sample's bulk density.

## Apparatus

We use an epoxy-filled needle probe with a 1.6 mm outer diameter stainless-steel sheath containing a 4 k $\Omega$  thermistor and a heater wire loop with resistance  $R = 350 \Omega/\text{m}$ . The 160-mm-long probe penetrates an o-ring seal in the endcap of a stainless-steel vessel with a maximum working pressure of 105 MPa (Fig. 1). The pressure vessel is immersed in a denatured alcohol bath connected to a bath circulator, which maintains isothermal conditions at selected temperatures during the experiment ( $\pm 0.002^\circ\text{C}$ ).

The sample is jacketed in a 0.1-mm-thick Teflon liner, and can be radially compacted around the axial probe by pressurizing the space surrounding the liner with silicone oil using an automated pump to 34.5 MPa, and by a manual pump for compaction pressures up to 105 MPa. During a thermal property measurement, a DC current

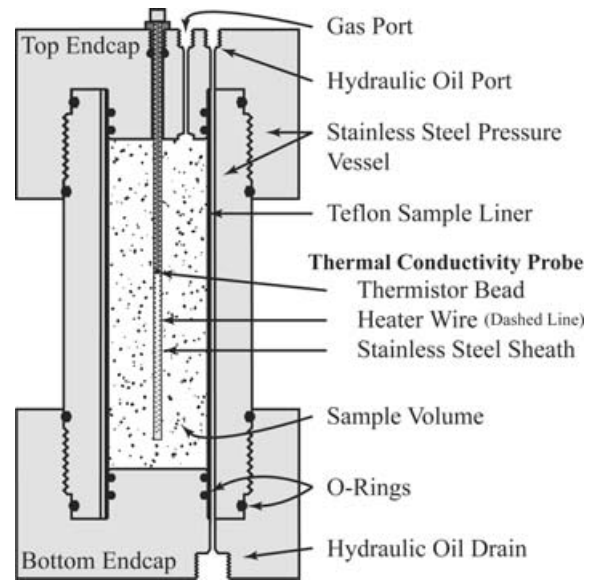


**Figure 1.** Pressure vessel and needle probe schematic, with needle probe enlarged to show detail. Probe diameter is 1.6 mm, sample diameter is 41 mm, sample length is 133 mm, and the thermistor is located 50 mm below the top of the sample. Needle probe seals against an o-ring in the top end cap and is held in place with an external brace (not pictured).

source supplies a constant current to the heater wire while a data acquisition unit logs the current source and thermistor output.

## Sample preparation

We form pure  $\text{CH}_4$  hydrate directly in the measurement chamber by slowly heating granular (180–250  $\mu\text{m}$ )  $\text{H}_2\text{O}$  ice in a pressurized  $\text{CH}_4$  atmosphere, as described by Stern *et al.* (1996, 1998). This reproducible technique produces  $\text{CH}_4$  hydrate with bulk composition:  $\text{CH}_4 \cdot (5.89 \pm 0.01) \cdot \text{H}_2\text{O}$  when quenched after high-pressure synthesis (Stern *et al.* 2000).

We check for full reaction to  $\text{CH}_4$  hydrate by lowering the sample temperature below the ice point. If more than 2 per cent of the initial seed ice persists as water, a pressure transducer detects the pore gas pressure increase due to water expanding while freezing. Heat liberated when water freezes provides an additional, more sensitive indicator of unreacted water near the thermistor bead. In this work, ice volumes are below our detection levels.

Following hydrate synthesis, the sample porosity is  $\sim 34$  per cent. To reduce porosity, silicone oil is pumped between the vessel walls and Teflon sample liner, holding a compaction pressure of  $\sim 102$  MPa at  $14.4^\circ\text{C}$  for 4 days. Cryogenic SEM images of the recovered sample show dense, fine-grained hydrate ( $\sim 5$  to  $50 \mu\text{m}$  grain size). Porosity is difficult to assess from SEM images of the depressurized sample, but is expected to be less than 5 per cent based on previous experience with samples compacted axially at 105 MPa (Helgerud 2001). The consistency of this synthesis and compaction method is evident in our thermal property results, which show a sample-to-sample variability below 3 per cent for thermal conductivity. Thermal diffusivity and specific heat vary by  $\sim 5$  per cent.

Following compaction at  $14.4^\circ\text{C}$ , we measure the pressure dependence of  $\text{CH}_4$  hydrate thermal properties from 102 MPa down to our operating confining pressure of 31.5 MPa. This pressure ensures  $\text{CH}_4$  hydrate stability between  $-20^\circ\text{C}$  and  $17^\circ\text{C}$ .

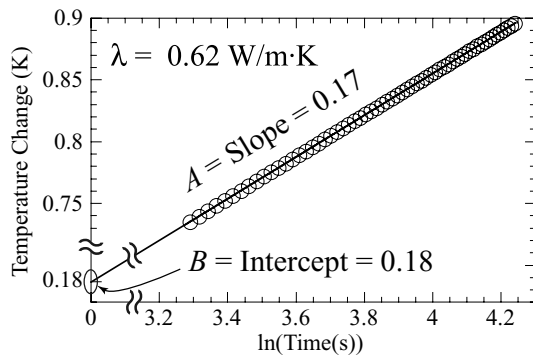


**Figure 2.** Measured temperature change for CH<sub>4</sub> hydrate at 9.6°C, showing every 20th data point of the nearly 900 points used in the linear fit. From this log time plot, thermal conductivity is calculated from the linear slope, *A*. The extrapolated linear intercept, *B*, is used in determining thermal diffusivity.

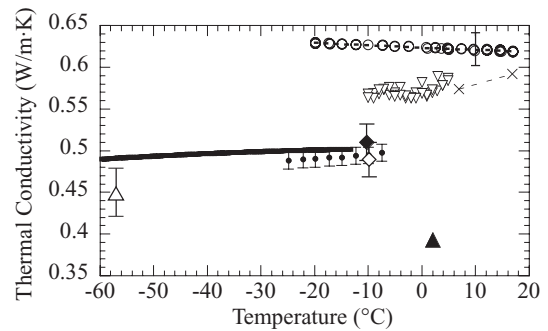
## RESULTS

### Thermal conductivity, $\lambda$

As required by eq. (1), heating the needle probe generates a temperature change in CH<sub>4</sub> hydrate that varies linearly with the natural log of time measured in seconds (Fig. 2). Using ~900 points in the Fig. 2 linear fit to obtain  $\lambda$  yields a stable, highly repeatable measure of  $\lambda$ , as shown in Fig. 3 (open circles, minimum of four separate measurements are plotted at each temperature). Variations at a given temperature are small relative to the sample-sample variability of nearly  $\pm 3$  per cent (plotted as an error bar in Fig. 3 at 10°C for our work). Linear temperature and pressure fits for  $\lambda$  are given in Tables 1 and 2. The dependencies are weak:  $\lambda$  changes only by 1.6 per cent between  $-20^\circ\text{C}$  and  $17^\circ\text{C}$ , and 1.5 per cent between 31.5 and 102 MPa.

Two potential sources of measurement error can be assessed directly from Fig. 3: sample contamination with unreacted H<sub>2</sub>O, and time-based changes in  $\lambda$  due to annealing or aging (Huang & Fan 2005). The smooth, linear transition in  $\lambda$  from temperatures below, to temperatures above the freezing point of water supports our assertion of insignificant levels of unreacted H<sub>2</sub>O in the system. Because  $\lambda_{\text{ice}}$  is ~4 times that of CH<sub>4</sub> hydrate (Sloan 1998; Waite *et al.* 2006), and  $\lambda_{\text{water}}$  is slightly less than that of CH<sub>4</sub> hydrate, unreacted H<sub>2</sub>O in the system causes a discontinuous step in thermal conductivity across the water/ice transition temperature. The lack of such a step in our results means the contribution of unreacted H<sub>2</sub>O is below our thermal property detection levels.

To assess aging effects, CH<sub>4</sub> hydrate thermal properties were measured in ~5°C steps from 15°C to  $-20^\circ\text{C}$ , then ~5°C steps from  $-17.5^\circ\text{C}$  to  $+17^\circ\text{C}$ , providing a complete profile with ~2.5°C increments. By cycling the temperature in this way, we verify the negative slope of  $\lambda$  with temperature is a material property of sI CH<sub>4</sub> hydrate, not an artefact of aging or annealing within the sample.



- sI Hydrate**
- Methane, This Work
  - ▽ Methane, Huang & Fan [2004]
  - △ Methane, Cook & Leaist [1983]
  - ◇ Ethylene-Oxide, Cook & Laubitz [1981]
- sII Hydrate**
- THF, Waite *et al.* [2006]
  - THF, Ross & Andersson [1982]
  - ◆ THF, Cook & Laubitz [1981]
  - ▲ Propane, Stoll & Bryan [1979]
- Water**
- × Weast [1987]

**Figure 3.** Temperature dependence of thermal conductivity for sI hydrates (open symbols), sII hydrates (closed symbols and heavy line) and water (crosses). The error bar at 10°C represents our sample-to-sample variability of  $\pm 0.02 \text{ Wm}^{-1} \text{ K}^{-1}$ . The thermal conductivity of methane hydrate is closer to water than ice; the latter has a thermal conductivity exceeding  $2.2 \text{ Wm}^{-1} \text{ K}^{-1}$  (Waite *et al.* 2006).

Variations in  $\lambda$  are less than 0.5 per cent between points taken at the beginning and end of the complete cycle.

Our measurements of  $\lambda$  are shown in Fig. 3 relative to published results for sI hydrates, sII hydrates and pure water. The data sets shown in Fig. 3 are measured at different pressures, but accounting for pressure differences does not remove the variability between data sets. As an example, our sI methane hydrate measurements are made at 31.5 MPa, whereas Huang & Fan (2004) operated at 2 MPa (inverted triangles). Based on our measured pressure dependence, our results should be decreased by  $\sim 0.003 \text{ Wm}^{-1} \text{ K}^{-1}$  ( $\sim 0.5$  per cent) to be directly comparable to the sI methane hydrate results from Huang & Fan (2004). Such a decrease, however, accounts for only ~5 per cent of the average difference between the two data sets. Ross & Andersson (1982) measured an even smaller pressure dependence of  $\sim 0.005$  per cent  $\text{MPa}^{-1}$  for  $\lambda$  in sII THF hydrate. We apply this pressure correction to their measurements at 100 MPa, lowering their results by  $0.0025 \text{ Wm}^{-1} \text{ K}^{-1}$  to obtain the solid line in Fig. 3 for comparison with the 2 MPa THF hydrate measurements by Waite *et al.* (2006) (solid circles in Fig. 3).

Variability between data sets shown in Fig. 3 is more likely controlled by measurement-specific factors; for brevity we focus only on CH<sub>4</sub> hydrate results. Hydrate purity is not well constrained in the

**Table 1.** CH<sub>4</sub> hydrate thermal property dependence on temperature, measured at 31.5 MPa confining pressure.

Temperature dependence fit equation	Temperature range
$\lambda \text{ (Wm}^{-1} \text{ K}^{-1}) = -(2.78 \pm 0.05) \cdot 10^{-4} \cdot T(^{\circ}\text{C}) + (0.62 \pm 0.02)$	$-20^\circ\text{C} - 17^\circ\text{C}$
$*\kappa \text{ (m}^2 \text{ s}^{-1}) = (5.04 \pm 0.02) \cdot 10^{-5}/T(\text{K}) + (1.25 \pm 0.05) \cdot 10^{-7}$	$1^\circ\text{C} - 17^\circ\text{C}$ (274–290 K)
$c_p \text{ (Jkg}^{-1} \text{ K}^{-1}) = (6.1 \pm 0.3) \cdot T(^{\circ}\text{C}) + (2160 \pm 100)$	$1^\circ\text{C} - 17^\circ\text{C}$

\*The  $T^{-1}$  dependence of the  $\kappa$  fit requires input temperatures in Kelvin.

**Table 2.** CH<sub>4</sub> hydrate thermal property dependence on pressure, measured at 14.4°C between 31.5 and 102 MPa confining pressure.

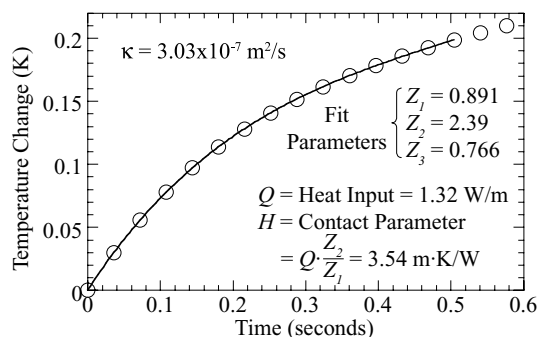
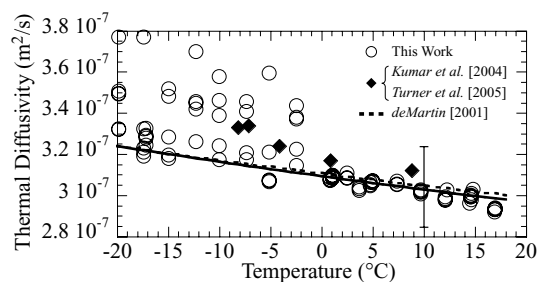
Pressure dependence fit equation
$\lambda$ (Wm <sup>-1</sup> K <sup>-1</sup> ) = (2.54 ± 0.06) · 10 <sup>-4</sup> · P(MPa) + (0.61 ± 0.02)
$\kappa$ (m <sup>2</sup> s <sup>-1</sup> ) = (2.87 ± 0.08) · 10 <sup>-10</sup> · P(MPa) + (3.1 ± 0.2) · 10 <sup>-7</sup>
$c_p$ (Jkg <sup>-1</sup> K <sup>-1</sup> ) = (3.30 ± 0.06) · P(MPa) + (2140 ± 100)

work of Cook & Leaist (1983) (open triangle at -57°C), who estimate 43 per cent of their hydrate dissociated into ice, and calculate  $\lambda_{\text{hydrate}}$  assuming  $\lambda_{\text{ice}}$  to be 2.65 Wm<sup>-1</sup> K<sup>-1</sup> at -57°C. Huang & Fan (2004) (inverted open triangles) formed methane hydrate by combining methane gas with a solution of water and sodium dodecyl sulphate (SDS). They removed gas-filled porosity by compacting their sample with a 2 MPa load. CH<sub>4</sub> hydrate resists compaction, requiring a load exceeding 100 MPa to achieve full compaction in acoustic wave speed measurements by Helgerud (2001). We observe a rapid thermal conductivity increase due to porosity reduction for compaction pressures up to 35–40 MPa, leading us to believe our measurements are higher than those of Huang & Fan (2004) at least in part because our final compaction pressure of 102 MPa reduced the gas-filled, low-thermal conductivity porosity below the level obtained using a 2 MPa compaction load by Huang & Fan (2004).

### Thermal diffusivity, $\kappa$

Unlike  $\lambda$ , for which approximately 900 data points covering over a minute of heating time are used to obtain the necessary fit parameters, transient heating governed by  $\kappa$  requires a non-linear fit in eq. (5) to fewer than 20 data points spanning the initial few tenths of a second of heating (Fig. 4). The small number of data points and non-linear fit required to calculate  $\kappa$  from  $H$  (eqs 3 and 4) and  $\Delta T$  (eq. 5) results in a larger fractional uncertainty in  $\kappa$  relative to  $\lambda$ . The uncertainty in  $\kappa$  increases as the acquisition rate, and hence the number of available data points, decreases. This point is illustrated in Fig. 5 (open circles). Above 0°C, the needle probe's thermistor resistance drops below 10 k $\Omega$ , allowing a data acquisition rate of 27.8 meas. s<sup>-1</sup>, compared to 18.2 meas. s<sup>-1</sup> below 0°C. Though the scatter in repeated measurements above 0°C can reach  $\pm 3$  per cent, the measurement uncertainty is controlled by the sample-to-sample variability of approximately  $\pm 7$  per cent (error bar in Fig. 5 at 10°C for our work).

In contrast to our technique, data to which we compare our results are obtained by measuring the travel time of a heating (or cooling)

**Figure 4.** Transient initial temperature change for CH<sub>4</sub> hydrate at 9.6°C. The short duration of transient heating limits data available (open circles) for the non-linear fit (solid curve) required for the thermal contact parameter,  $H$  (eq. 5). Low data acquisition rates further limit the number of data points, reducing the precision with which  $H$  and  $\kappa$  can be estimated (see Fig. 5).**Figure 5.** Temperature dependence of thermal diffusivity for sI CH<sub>4</sub> hydrate. Improved uncertainty in our measurements (open circles) above 0°C is due to a 50 per cent increase in our data acquisition rate for measurements above 0°C. The error bar at 10°C represents our sample-to-sample variability of  $\pm 0.2 \times 10^{-7}$  m<sup>2</sup> s<sup>-1</sup>. The solid line is a fit through our data above 0°C (see Table 2). The dotted line is an extrapolated fit from deMartin's (2001) -128°C to -106°C data. The samples of Kumar *et al.* (2004) and Turner *et al.* (2005) include  $\sim 30$  per cent methane gas-filled porosity (diamonds).

front between temperature sensors with a known separation within a sample. The dotted line in Fig. 5 is an extrapolated fit to measurements made between -128°C and -106°C (145 to 167 K) at 7 MPa by deMartin (2001) on compacted CH<sub>4</sub> hydrate. The hydrate is formed from granular ice, according to the method of Stern *et al.* (1996), then axially compacted to  $\sim 105$  MPa at -20°C using the apparatus described by Helgerud (2001). The fit for the deMartin sample is given by  $\kappa_{\text{deMartin}} = 1.43 \times 10^{-7} + 4.58 \times 10^{-5} T^{-1}$  (K), where  $T^{-1}$  (K) is the inverse of temperature in Kelvin. The solid curve is a fit of the same form calculated from our measurements above 0°C (see Table 1). Agreement between our fit and that of deMartin (2001) suggests  $\kappa$  measurements made with a low data acquisition rate do not scatter equally above and below the expected value. The lowest values in the scatter appear to best represent  $\kappa$  in CH<sub>4</sub> hydrate.

Solid diamonds in Fig. 5 represent results for porous CH<sub>4</sub> hydrate measured between 4.35 and 7.65 MPa by Kumar *et al.* (2004), republished with the addition of a data point in Turner *et al.* (2005). Their hydrate is formed from granular ice, according to the method of Stern *et al.* (1996). Taking their initial volume fraction of ice to be 0.6 (Turner, personal communication, 2006), the density of ice and an empty sI hydrate lattice to be 917 and 790 kg m<sup>-3</sup>, respectively (Dvorkin *et al.* 2000), the resulting hydrate fraction is  $\sim 0.7$  with a porosity of  $\sim 30$  per cent. Agreement between their porous and our compacted hydrate results can be understood from eq. (6). Since  $c_p$  is the heat capacity per unit mass of material, eliminating gas-filled porosity insignificantly changes the sample mass and  $c_p$  remains essentially constant. Eliminating low-density, low-thermal conductivity gas-filled porosity increases both  $\rho$  and  $\lambda$ , the effects of which tend to cancel each other out in eq. 6, leaving  $\kappa$  only weakly dependent on gas-filled porosity.

Agreement between data sets plotted in Fig. 5, obtained using three different measurement techniques, provides a consensus result for  $\kappa$  in sI methane hydrate. Temperature and pressure fits for  $\kappa$ , based on our results above 0°C, are given in Tables 1 and 2. The dependencies are stronger than for  $\lambda$ , with  $\kappa$  decreasing 7.4 per cent between -20°C and 17°C, and 15.1 per cent between 31.5 and 102 MPa.

### Specific heat, $c_p$

We calculate  $c_p$  from our measurements of  $\lambda$  and  $\kappa$  using eq. (6), for which density,  $\rho$ , is the only additional parameter required. We calculate  $\rho$  from the unit cell volume,  $V_o$ , and unit cell mass, assuming

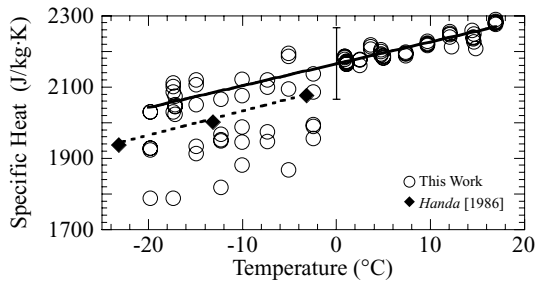


**Figure 6.** Temperature dependence of specific heat for sI CH<sub>4</sub> hydrate. Uncertainty in our measurements (open circles) is due primarily to the uncertainty in thermal diffusivity (see Fig. 5). The error bar at 0°C represents our sample-to-sample variability of  $\pm 100 \text{ J kg}^{-1} \text{ K}^{-1}$ . The solid line is a fit through our data above 0°C (see Table 1). The dotted line is a cubic fit presented by Handa (1986) for CH<sub>4</sub> hydrate measured between  $-188^\circ\text{C}$  and  $-3^\circ\text{C}$  (diamonds).

a stoichiometry of CH<sub>4</sub> · nH<sub>2</sub>O, with  $n = 5.89$  (see Section 2.3). CH<sub>4</sub> hydrate has a cubic structure, so  $V_o$  is taken as the cube of the lattice parameter  $a_f$ , measured as a function of temperature by Shpakov *et al.* (1998). Extrapolating to our measurement temperature range of  $-20^\circ\text{C}$  to  $+17^\circ\text{C}$  yields:

$$\rho_{\text{hydrate}}(\text{kg m}^{-3}) = 926.45 - 0.239 \cdot T(^{\circ}\text{C}) - 3.7310^{-4} \cdot T(^{\circ}\text{C})^2. \quad (7)$$

We assume  $n = 5.89$  because our measurement ranges are well within the pressure and temperature stability field for CH<sub>4</sub> hydrate. For samples annealed along the equilibrium boundary,  $n$  evolves slightly to CH<sub>4</sub>·(5.99 ± 0.07)H<sub>2</sub>O (Circone *et al.* 2005). Density does not depend strongly on the choice of  $n$  however, decreasing by less than 0.25 per cent for an  $n$  of 6 rather than 5.89.

Because  $c_p$  is calculated from  $\kappa$ , the scatter in  $c_p$  is proportional to the scatter in  $\kappa$ , resulting in a measurement repeatability above 0°C of  $\pm 3$  per cent, and a sample-to-sample variability of  $\pm 5$  per cent (plotted as an error bar in Fig. 6 at 0°C). When the data acquisition rate is low, high values of  $c_p$  are the most representative values (see Fig. 6, below 0°C). These high value  $c_p$  data points are the points calculated via eq. (6) from the low values of  $\kappa$  shown in the previous section to be the most representative for thermal diffusivity. We calculate our linear fit from points above 0°C (see Tables 1 and 2). Between  $-20$  and  $17^\circ\text{C}$ ,  $c_p$  increases 11.1 per cent. At  $14.4^\circ\text{C}$ ,  $c_p$  increases by 5.9 per cent between 31.5 and 102 MPa.

Handa (1986) assumed a hydrate stoichiometry of CH<sub>4</sub> · 6H<sub>2</sub>O, and measured a specific heat,  $c_{p\text{Handa}}$ , given by:

$$c_{p\text{Handa}}(\text{J kg}^{-1} \text{ K}) = 2100 - 7.07 \cdot T(^{\circ}\text{C}) + 1.2310^{-2} \cdot T(^{\circ}\text{C})^2 + 5.08 \times 10^{-2} \cdot T(^{\circ}\text{C})^3. \quad (8)$$

Measurement pressure differences between the 31.5 MPa used in our work and the  $\sim 3$  MPa used by Handa (1986) account for half the 4 per cent discrepancy between our derived values of  $c_p$  and Handa's direct measurement of  $c_p$  via precision calorimetry. Based on our sample-to-sample variability of  $\pm 5$  per cent, however, differences between our measurements and those of Handa are not considered significant.

## APPLICATION TO NATURAL SYSTEMS

We report thermal properties of pure CH<sub>4</sub> hydrate, but CH<sub>4</sub> hydrate often exists naturally as a pore-space constituent in a formation containing both sediment and water. To provide a sense of the hydrate

quantity needed to significantly alter the thermal properties of an otherwise water-saturated formation, we focus on two controlling parameters: sediment porosity,  $\phi$ , and hydrate saturation of that pore space,  $S_h$ . Typical porosities and hydrate saturations for five representative environments are listed in Table 3.

The Mallik 5L-38 gas hydrate research well, located in a permafrost region of the northern coast of Canada's Northwest Territory, was the site of a 2002 production test for obtaining methane from hydrate, and represents a high hydrate saturation end-member case (Dallimore & Collett 2005). The Cascadia Margin, an accretionary margin system offshore Vancouver, Canada (Expedition 311 Scientists 2005), and the Congo continental slope (Sultan *et al.* 2004), both have near-surface hydrate with indicators of gas venting to the seafloor. Blake Ridge, a passive margin offshore South Carolina, USA, has a well-developed seismic indicator of free gas underlying hydrate-bearing sediment through which logging indicates peak hydrate saturations comparable to the Congo continental slope, and background hydrate saturations of only a few percent (Helgerud *et al.* 1999).

We further simplify the comparison of hydrate effects on thermal properties in natural systems by assuming the formation temperature is 8°C, the temperature used in studies of the Mallik 5L-38 well (Moridis *et al.* 2005). The host sediment is assumed to be quartz, with density  $\rho_{\text{quartz}} = 2650 \text{ kg m}^{-3}$ , thermal conductivity  $\lambda_{\text{quartz}} = 8 \text{ W m}^{-1} \text{ K}$  (Beck 1976), and specific heat  $c_{p\text{quartz}} = 943 \text{ J kg}^{-1} \text{ K}$  (Sultan *et al.* 2004). The pore fluid is assumed to be pure water. Ignoring effects of pressure and salinity, the density and thermal properties of water are given as functions of temperature,  $T(^{\circ}\text{C})$ , by (Weast 1987):

$$\rho_{\text{water}}(\text{kg m}^{-3}) = 999.9 + 5.330 \times 10^{-2} \cdot T(^{\circ}\text{C}) - 6.834 \times 10^{-3} \cdot T(^{\circ}\text{C})^2, \quad (9)$$

$$\lambda_{\text{water}}(\text{W m}^{-1} \text{ K}^{-1}) = 0.562 + 1.75 \times 10^{-3} \cdot T(^{\circ}\text{C}), \quad (10)$$

$$\kappa_{\text{water}}(\text{m}^2 \text{ s}^{-1}) = 1.33 \times 10^{-7} + 5.28 \times 10^{-10} \cdot T(^{\circ}\text{C}) - 3.63 \times 10^{-12} \cdot T(^{\circ}\text{C})^2 + 1.03 \times 10^{-13} \cdot T(^{\circ}\text{C})^3 - 1.15 \times 10^{-15} \cdot T(^{\circ}\text{C})^4, \quad (11)$$

$$c_{p\text{water}}(\text{J kg}^{-1} \text{ K}^{-1}) = 4217 - 3.79 \cdot T(^{\circ}\text{C}) + 0.157 \times 10^{-3} \cdot T(^{\circ}\text{C})^2 - 3.71 \times 10^{-3} \cdot T(^{\circ}\text{C})^3 + 4.29 \times 10^{-5} \cdot T(^{\circ}\text{C})^4. \quad (12)$$

For our assumed hydrate stoichiometry of CH<sub>4</sub> · 5.89H<sub>2</sub>O, we calculate density as explained previously using hydrate lattice volume data from Shpakov *et al.* (1998). CH<sub>4</sub> hydrate thermal properties are taken from Table 1.

## Thermal conductivity

The relation between heat flow and geothermal gradient is determined by the effective thermal conductivity,  $\lambda_{\text{eff}}$ . Revil (2000) provides a comprehensive appraisal of mixing models and presents a robust model accounting for many of the shortcomings in previously existing models. For a sand + water + CH<sub>4</sub> hydrate system,  $\lambda_{\text{eff}}$  is calculated from the mixing model by (Revil 2000):

$$\lambda_{\text{eff}} = \frac{\lambda_f}{\xi} \left[ \xi \Theta + \frac{1}{2} (1 - \Theta) (1 - \Theta + \sqrt{(1 - \Theta)^2 + 4\xi \Theta}) \right], \quad (13)$$

**Table 3.** Typical sediment porosity,  $\phi$ , and hydrate saturation,  $S_h$ , for sites in comparative study.

Site	$\phi$ (%)	$S_h$ (%)
Mallik 5L-38 <sup>a</sup>	35	80
Cascadia X311 Site 1326 <sup>b</sup>	50	50
Congo Continental Slope <sup>c</sup>	74	10
Blake Ridge Site 995 (peak)	60 <sup>d</sup>	9 <sup>e</sup>
Blake Ridge Side 995 (background)	60 <sup>d</sup>	3 <sup>e</sup>

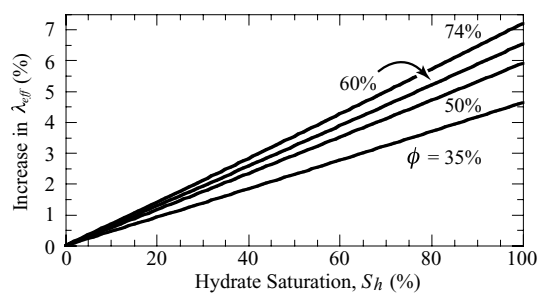
<sup>a</sup>Collett *et al.* (2005).<sup>b</sup>Expedition 311 Scientists (2005).<sup>c</sup>Sultan *et al.* (2004).<sup>d</sup>Guerin *et al.* (1999).<sup>e</sup>Helgerud *et al.* (1999).

where  $\Theta = \frac{\lambda_s}{\lambda_f}$ , and  $\xi = \phi \left( \frac{m}{1-m} \right)$ . The subscripts  $s$  and  $f$  refer to sand and fluid, respectively,  $\phi$  is sediment porosity, and the cementation exponent  $m$  is taken from Revil (2000) to be 2.

For the purpose of comparing porosity and hydrate saturation effects on thermal properties in sediment, hydrate is assumed to be part of the pore fluid, and the two-phase mixing law from Revil (2000) is applied twice to obtain  $\lambda_{\text{eff}}$  for hydrate-bearing sediment. In step one, the effective thermal conductivity of the pore fluid is calculated from eq. 13 by assuming hydrate is the solid phase, water is the pore fluid, and  $\phi$  is the volume fraction of water relative to hydrate,  $(1 - S_h)$ . In step two, eq. (13) is applied assuming  $\lambda_s$  is the thermal conductivity of quartz, and  $\lambda_f$  is the effective thermal conductivity calculated in step 1. Porosity is given in Table 3.

Of the three thermal properties discussed here, methane hydrate and water are most alike in thermal conductivity. Fig. 7 shows the percent increase in  $\lambda$  for water- and hydrate-bearing sand with hydrate saturation,  $S_h$ , above that of sand saturated with water alone. Each curve represents a site porosity from Table 3.

The maximum thermal conductivity increase in a hydrate-saturated sand relative to a water-saturated sand is only  $\sim 8$  per cent, even in a high-porosity, surface-sediment system such as the Congo continental slope with 74 per cent porosity. For more typical porosities and hydrate saturations, the effect is even smaller. By comparison, Hennings & Huenges (2005) state that 7 per cent variations in  $\lambda_{\text{eff}}$  are not measurable with available geothermal data. A study by Grevermeyer & Villinger (2001) of Ocean Drilling Program boreholes in marine hydrate systems similarly concludes that geothermal gradient measurement errors are  $\sim 10$  per cent at best, and the contribution of CH<sub>4</sub> hydrate to  $\lambda_{\text{eff}}$  of hydrate-bearing sediment is insignificant.

**Figure 7.** Change in effective thermal conductivity,  $\lambda_{\text{eff}}$ , as pore water is replaced by methane hydrate. Increasing sediment porosity,  $\phi$  (see Table 3), accentuates hydrate's effect on  $\lambda_{\text{eff}}$ , but the effect is less than  $\sim 8$  per cent even in fully-hydrate saturated, high-porosity sediment. Hydrate does not significantly impact sediment thermal conductivity.

## Thermal diffusivity

Thermal diffusivity is important when describing how a thermal front moves through a system. Briaud & Chaouch (1997) model temperature increases in sediment occurring when high-temperature hydrocarbons are drawn up through a well to the seafloor. For a given distance from the well, they find the time required to raise the formation temperature to a given value is proportional to  $1/\kappa_{\text{eff}}$ , where  $\kappa_{\text{eff}}$  is the effective thermal diffusivity. The thermal diffusivity of CH<sub>4</sub> hydrate is more than twice that of water, meaning  $\kappa_{\text{hydrate}}$  has a greater effect on  $\kappa_{\text{eff}}$  than  $\lambda_{\text{hydrate}}$  has on  $\lambda_{\text{eff}}$ .

In the absence of systematic studies of thermal diffusivity mixing models, we quantify the effect of  $\kappa_{\text{hydrate}}$  on  $\kappa_{\text{eff}}$  using the definition of thermal diffusivity from whence we derived  $c_p$  in eq. (6) (Kittel & Kroemer 1980):

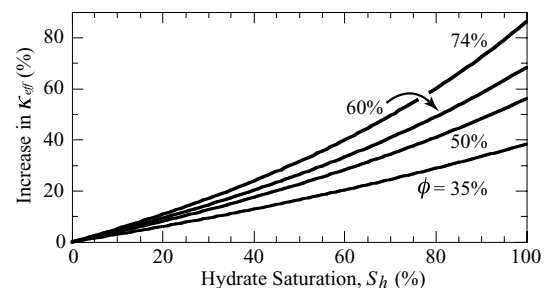
$$\kappa \equiv \frac{\lambda}{\rho \cdot c_p} \quad (14)$$

To calculate  $\kappa_{\text{eff}}$  of a sand + water + CH<sub>4</sub> hydrate system, we use the effective thermal conductivity,  $\lambda_{\text{eff}}$ , from eq. (13). The effective density,  $\rho_{\text{eff}}$ , and specific heat  $c_{\text{peff}}$ , are calculated in section 4.3 (eqs 15 and 16, respectively).

Ignoring the effects of methane hydrate and assuming pores are saturated only with water can result in  $> 10$  per cent overestimates of the heating time in reservoirs with only 35 per cent hydrate saturation of 35 per cent porosity (Fig. 8). In porous, near-surface sediments of the Cascadia Margin or Congo continental slope, hydrate saturations of only 19–22 per cent result in  $> 10$  per cent reductions in heating times relative to sediment with no hydrate. Hydrate should be accounted for in transient heat flow applications such as safety assessments for drilling into or through hydrate-bearing sediment (Ji *et al.* 2003; Pooladi-Darvish 2004).

## Specific heat

Specific heat, a measure of the heat stored in the system, is a controlling parameter during hydrate dissociation. Hydrate dissociation is an endothermic process, and the dissociation rate can be limited if insufficient heat is available at the dissociation front (Hong & Pooladi-Darvish 2005). The specific heat of CH<sub>4</sub> hydrate is less than half that of water, meaning the presence of hydrate can significantly lower the specific heat of hydrate-bearing sediment relative to water-saturated sediment.

**Figure 8.** Change in effective thermal diffusivity,  $\kappa_{\text{eff}}$ , as pore water is replaced by methane hydrate. Even for sediment porosities,  $\phi$  (see Table 3), and hydrate saturations,  $S_h$ , of 35 per cent, methane hydrate increases  $\kappa_{\text{eff}}$  by more than 10 per cent. Hydrate can significantly increase the propagation rate of a thermal front from a heat source such as a conventional hydrocarbon well, potentially reducing nearby sediment strength (Briaud & Chaouch 1997).

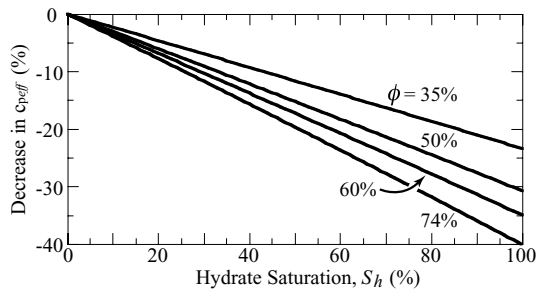


**Figure 9.** Change in effective specific heat,  $c_{p,eff}$ , as pore water is replaced by methane hydrate. For sediment porosities,  $\phi$  (see Table 3), exceeding 35 per cent, and hydrate saturations,  $S_h$ , above 40 per cent, methane hydrate decreases  $c_{p,eff}$  by more than 10 per cent. Hydrate can significantly decrease the heat stored in hydrate-bearing sediment that is available for hydrate dissociation, reducing dissociation rates. This is particularly apparent at the high hydrate saturation characteristic of likely targets for methane production from hydrate and must be accounted for in production models (Moridis *et al.* 2005).

Quantifying the effect of  $c_{p,hydrate}$  on  $c_{p,eff}$  requires the total density,  $\rho_{eff}$ :

$$\rho_{eff}(\text{kg m}^{-3}) = \rho_{rock} \cdot (1 - \phi) + \rho_{water} \cdot \phi \cdot (1 - S_h) + \rho_{hydrate} \cdot \phi \cdot S_h, \quad (15)$$

where  $\phi$  is the porosity,  $S_h$  is the hydrate saturation of the pore space, and the subscript rock, water and hydrate refer to the host sediment, the pore water, and the  $\text{CH}_4$  hydrate, respectively. Using the same subscript convention, the formation's specific heat,  $c_{p,eff}$  is given by (Sultan *et al.* 2004):

$$c_{p,eff}(\text{J kg}^{-1} \text{K}^{-1}) = c_{p,rock} \cdot \frac{(1 - \phi) \cdot \rho_{rock}}{\rho_{eff}} + c_{p,water} \cdot \frac{(1 - S_h) \cdot \phi \cdot \rho_{water}}{\rho_{eff}} + c_{p,hydrate} \cdot \frac{S_h \cdot \phi \cdot \rho_{hydrate}}{\rho_{eff}}. \quad (16)$$

The rock density in each example is given as that of quartz,  $2650 \text{ kg m}^{-3}$ . For the purpose of comparison,  $c_{p,rock}$  in all three examples will be taken as  $943 \text{ J kg}^{-1} \text{ K}^{-1}$  (Sultan *et al.* 2004). The properties of water are given in eqs 9–12.  $\text{CH}_4$  hydrate density is calculated from eq. 7, and its specific heat is taken from Table 1. Relative to a water-saturated sand, the percent decrease in  $c_{p,eff}$  is plotted as a function of hydrate fraction in Fig. 9. The porosities are those given in Table 3.

Candidate sites for producing  $\text{CH}_4$  from hydrate, such as the hydrate-bearing layers used for production testing in the Mallik 5L-38 well, with  $\sim 35$  per cent porosity  $\sim 80$  per cent saturated with methane hydrate (Collett *et al.* 2005), are particularly affected by the presence of hydrate. This effect is recognized in the Mallik 5L-38 production test modelling by Kurihara *et al.* (2005) and Moridis *et al.* (2005), but the effect is  $> 10$  per cent even for moderate hydrate saturations.

Comparing Figs 8 and 9, the impact of  $\text{CH}_4$  hydrate on  $\kappa_{eff}$  appears to be about twice the impact on  $c_{p,eff}$ , even though both properties differ from that of water by approximately a factor of two. This is due largely to an artefact of the comparison. Figs 8 and 9 are plots of a property's percentage change relative to water-saturated sediment. For thermal diffusivity, the diffusivity increase in hydrate-bearing sediment is divided by the smaller diffusivity of water-saturated sediment. For specific heat, however, the decrease is divided by the larger specific heat of water-saturated sand, muting the impact

of hydrate on the fractional decrease of specific heat with hydrate saturation. The magnitude of change for specific heat would be similar to that for thermal diffusivity if Fig. 9 were plotted as the percentage change in specific heat relative to hydrate-saturated sand when water replaces hydrate in the pore space.

## CONCLUSIONS

Our simultaneous measurements of  $\lambda$ ,  $\kappa$  and  $c_p$  provide a comprehensive thermal property description for pure sl  $\text{CH}_4$  hydrate that closely agrees with, and ties together, the limited available results measured using other techniques. With a suitably high data acquisition rate, this needle probe technique can be used in tests of unconsolidated sediment and other materials that can be penetrated or formed in close contact with the probe.

Relative to pore water, the contribution of hydrate to thermal conductivity in hydrate-bearing sediments is small, and likely not detectable in field measurements. For sediment porosities exceeding  $\sim 30$  per cent containing hydrate saturations exceeding  $\sim 10$  per cent, however, hydrate's contribution to thermal diffusivity and specific heat can be significant, particularly in hydrocarbon production and sediment stability applications for which safety and economic viability issues must be addressed.

## ACKNOWLEDGMENTS

This work was supported by the Gas Hydrate Project of the U.S. Geological Survey's Coastal and Marine Geology Program, in addition to Department of Energy contract DE-AI21-92MC29214. The manuscript benefited significantly from discussions with Drs C. Ruppel and R. Williams.

## REFERENCES

- Beck, A.E., 1976. An improved method of computing the thermal conductivity of fluid-filled sedimentary rocks, *Geophysics*, **41**, 133–144.
- Blackwell, J.H., 1954. A transient-flow method for determination of thermal constants of insulating materials in bulk, *J. app. Phys.*, **25**(2), 137–144.
- Briaud, J.L. & Chaouch, A., 1997. Hydrate melting in soil around hot conductor, *Journal of Geotechnical and Geoenvironmental Engineering*, **123**(7), 645–653.
- Circone, S., Kirby, S.H., & Stern, L.A., 2005. Direct Measurement of Methane Hydrate Composition along the Hydrate Equilibrium Boundary, *J. Phys. Chem. B*, **109**, 9468–9475.
- Collett, T.S., 1995. Gas hydrate resources of the United States. In: D. L. Gautier, & G. L. Dolton (Editors), *National Assessment of US Oil & Gas Resources (CD-ROM)*, pp. 78 + CD.
- Collett, T.S., Lewis, R.E., & Dallimore, S.R., 2005. Mallik 5L-38 gas hydrate production research well downhole well-log and core montages. In: S.R. Dallimore & T.S. Collett (Editors), *Scientific Results From The Mallik 2002 Gas Hydrate Production Research Well Program, Mackenzie Delta, Northwest Territories, Canada*. Geological Survey of Canada, Bulletin 585.
- Cook, J.G. & Laubitz, M.J., 1981. The thermal conductivity of two clathrate hydrates, *Proc. 17th Int. Thermal Conductivity Conf.*, pp. 13.
- Cook, J.G. & Leaist, D.G., 1983. An exploratory study of the thermal conductivity of methane hydrates, *Geophys. Res. Lett.*, **10**(5), 397–399.
- Dallimore, S.R. & Collett, T.S., 2005. Summary and implications of the Mallik 2002 gas hydrate production research well program. In: S.R. Dallimore & T.S. Collett, *Scientific Results from the Mallik 2002 Gas Hydrate Production Research Well Program, Mackenzie Delta, Northwest Territories, Canada*. Geological Survey of Canada, Bulletin 585.

- deMartin, B.J., 2001. Laboratory measurements of the thermal conductivity and thermal diffusivity of methane hydrate at simulated in situ conditions. Masters Thesis, Georgia Institute of Technology, Atlanta, GA, 135 pp.
- Dickens, G.R., O'Neil, J.R., Rea, D.K. & Owen, R.M., 1995. Dissociation of oceanic methane hydrates as a cause of the carbon isotope excursion at the end of the Paleocene, *Paleoceanography*, **10**(6), 965–972.
- Dvorkin, J., Helgerud, M.B., Waite, W.F., Kirby, S.H. & Nur, A., 2000. Introduction to physical properties and elasticity models. In: M.D. Max (ed), *Natural Gas Hydrate In Oceanic and Permafrost Environments*. Kluwer Academic Publishers, Dordrecht, Netherlands (NLD), pp. 245–260.
- Expedition 311 Scientists, 2005. Cascadia margin gas hydrates. IODP Preliminary Reports, 311: doi:10.2204/iodp.pr.311.2005.
- Grevemeyer, I. & Villinger, H., 2001. Gas hydrate stability and the assessment of heat flow through continental margins, *Geophys. J. Int.*, **145**(3), 647–660.
- Guerin, G., Goldberg, D. & Meltser, A., 1999. Characterization of in situ elastic properties of gas hydrate-bearing sediments on the Blake Ridge, *J. geophys. Res.*, **104**(B8), 17781–17795.
- Hammerschmidt, U., 2005. Simultaneous Measurement of Thermal Conductivity, Thermal Diffusivity, and Volumetric Specific Heat, *Thermal Conductivity*, **27**, 313–327.
- Handa, Y.P., 1986. Compositions, enthalpies of dissociation, and heat capacities in the range 85 to 270 K for clathrate hydrates of methane, ethane, and propane, and enthalpy of dissociation of isobutane hydrate, as determined by a heat-flow calorimeter, *J. Chem. Thermodynamics*, **18**, 915–921.
- Helgerud, M.B., 2001. Wave speeds in gas hydrate and sediments containing gas hydrate: a laboratory and modeling study. Doctoral Thesis, Stanford University, Palo Alto, <http://srb.stanford.edu/Theses/Helgerud.82.pdf>, 251 pp.
- Helgerud, M.B., Dvorkin, J., Nur, A., Sakai, A. & Collett, T., 1999. Elastic-wave velocity in marine sediments with gas hydrates: effective medium modeling, *Geophys. Res. Lett.*, **26**(13), 2021–2024.
- Henningses, J. & Huenges, E., 2005. In situ thermal conductivity of gas-hydrate-bearing sediments of the Mallik 5L-38 well, *J. geophys. Res.*, **110**, B11206, doi:10.1029/2005JB003734.
- Hong, H. & Pooladi-Darvish, M., 2005. Numerical study of constant-rate gas production from in situ gas hydrate by depressurization. In: S.R. Dallimore & T.S. Collett (Editors), *Scientific Results from the Mallik 2002 Gas Hydrate Production Research Well Program, Mackenzie Delta, Northwest Territories, Canada*. Geological Survey of Canada, Bulletin 585.
- Huang, D. & Fan, S., 2004. Thermal conductivity of methane hydrate formed from sodium dodecyl sulfate solution, *Journal of Chemical and Engineering Data*, **49**, 1479–1482.
- Huang, D. & Fan, S., 2005. Measuring and modeling thermal conductivity of gas hydrate-bearing sand, *J. geophys. Res.*, **110**, B01311, doi:10.1029/2004JB003314.
- Ji, C., Ahmadi, G. & Smith, D.H., 2003. Constant rate natural gas production from a well in a hydrate reservoir, *Energy Conversion and Management*, **44**, 2403–2423.
- Kerr, R.A., 2004. Gas hydrate resource: smaller but sooner, *Science*, **303**, 946–947.
- Kittel, C. & Kroemer, H., 1980. *Thermal Physics*. pp. 473 W. H. Freeman & Co., New York.
- Kumar, P., Turner, D. & Sloan, E.D., 2004. Thermal diffusivity measurements of porous methane hydrate and hydrate-sediment mixtures, *J. geophys. Res.*, **109**, B01207, doi:10.1029/2003JB002763.
- Kurihara, M., et al., 2005. Analysis of the JAPEX/JNOC/GSC et al. Mallik 5L-38 gas hydrate thermal-production test through numerical simulation. In: S.R. Dallimore & T.S. Collett (Editors), *Scientific Results from the Mallik 2002 Gas Hydrate Production Research Well Program, Mackenzie Delta, Northwest Territories, Canada*. Geological Survey of Canada, Bulletin 585.
- Kvenvolden, K.A., 2000. Natural gas hydrate; introduction and history of discovery. In: M.D. Max (Editors), *Natural Gas Hydrate In Oceanic and Permafrost Environments*. Kluwer Academic Publishers, Dordrecht, Netherlands (NLD), pp. 9–16.
- Moridis, G.J., Collett, T.S., Dallimore, S.R., Inoue, T. & Mroz, T., 2005. Analysis and interpretation of the thermal test of gas hydrate dissociation in the JAPEX/JNOC/GSC et al. Mallik 5L-38 gas hydrate production research well. In: S.R. Dallimore & T.S. Collett (Editors), *Scientific Results from the Mallik 2002 Gas Hydrate Production Research Well Program, Mackenzie Delta, Northwest Territories, Canada*. Geological Survey of Canada, Bulletin 585.
- Moridis, G.J. & Kowalsky, M.B., 2006. *Response of Oceanic Hydrate-Bearing Sediments to Thermal Stresses, Paper OTC 18193*, Offshore Technology Conference, Houston, Texas.
- Pooladi-Darvish, M., 2004. Gas production from hydrate reserves and its modeling, *J. Petrol.*, **56**(6), 65–71.
- Revil, A., 2000. Thermal conductivity of unconsolidated sediments with geophysical applications, *J. geophys. Res.*, **105**, 16749–16768.
- Ross, R.G. & Andersson, P., 1982. Clathrate and other solid phases in the tetrahydrofuran-water system: thermal conductivity and heat capacity under pressure, *Can. Journ. Chem.*, **60**, 881–892.
- Shpakov, V.P., Tse, J.S., Tulk, C.A., Kvamme, B. & Belosludov, V.R., 1998. Elastic moduli calculation and instability in structure I methane clathrate hydrate, *Chem. Phys. Lett.*, **282**(2), 107–114.
- Sloan, E.D., Jr., 1998. *Clathrate Hydrates of Natural Gases*. Marcel Dekker Inc., New York, 705 pp.
- Sloan, E.D., Jr., 2004. Introductory overview: hydrate knowledge development, *American Mineralogist*, **89**, 1155–1161.
- Stern, L.A., Kirby, S.H. & Durham, W.B., 1996. Peculiarities of methane clathrate hydrate formation and solid-state deformation, including possible superheating of water ice, *Science*, **273**(5283), 1843–1848.
- Stern, L., Kirby, S. & Durham, W., 1998. Polycrystalline methane hydrate: synthesis from superheated ice, and low-temperature mechanical properties, *Energy and Fuels*, **12**(2), 201–211.
- Stern, L., Kirby, S., Durham, W., Circone, S. & Waite, W., 2000. Laboratory synthesis of pure methane hydrate suitable for measurement of physical properties and decomposition behavior. In: M.D. Max (Editor), *Natural Gas Hydrate in Oceanic and Permafrost Environments*. Kluwer Academic Publishers, Netherlands, pp. 323–348.
- Stoll, R.D. & Bryan, G.M., 1979. Physical properties of sediments containing gas hydrates, *J. geophys. Res.*, **84**, 1629–1634.
- Sultan, N., et al., 2004. Dynamics of gas hydrate: case of the Congo continental slope, *Marine Geology*, **206**(1–4), 1–18.
- Turner, D.J., Kumar, P. & Sloan, E.D., 2005. New technique for hydrate thermal diffusivity measurements, *Int. J. Thermophysics*, **26**(6), 1681–1691.
- von Herzen, R.P. & Maxwell, A.E., 1959. The measurement of thermal conductivity of deep-sea sediments by a needle probe method, *J. geophys. Res.*, **84**, 1629–1634.
- Waite, W.F., Gilbert, L.Y., Winters, W.J. & Mason, D.H., 2006. Estimating thermal diffusivity and specific heat from needle probe thermal conductivity data, *Review of Scientific Instruments*, **77**, 044904, doi:10.1063/1.2194481.
- Weast, R.C., 1987. *CRC Handbook of Chemistry and Physics*. CRC Press, Inc., Boca Raton.
- Xu, W. & Germanovich, L.N., 2006. Excess pore pressure resulting from methane hydrate dissociation in marine sediments: a theoretical approach, *J. geophys. Res.*, **111**, B01104, doi:10.1029/2004JB003600.